HOKKAIDO UNIVERSITY

Title	Fabrication and characterization of GaAs quantum well buried in AlGaAs/GaAs heterostructure nanowires
Author(s)	Hayashida, Atsushi; Sato, Takuya; Hara, Shinjiro et al.
Citation	Journal of Crystal Growth, 312(24), 3592-3598 https://doi.org/10.1016/j.jcrysgro.2010.09.057
Issue Date	2010-12-01
Doc URL	https://hdl.handle.net/2115/44507
Type	journal article
File Information	JCG312-24_3592-3598.pdf

Hokkaido University Collection of Scholarly and Academic Papers : HUSCAP

Fabrication and characterization of GaAs quantum well buried in AlGaAs/GaAs heterostructure nanowires

Atsushi Hayashida [a], Takuya Sato [a], Shinjiro Hara [b],

Junichi Motohisa [a], Kenji Hiruma [a,b,*], and Takashi Fukui [a,b]

[a] Graduate School of Information Science and Technology,

Hokkaido University, North 14 West 9, Sapporo 060-0814, Japan

[b] Research Center for Integrated Quantum Electronics,

Hokkaido University, North 13 West 8, Sapporo 060-8628, Japan

*E-mail: hiruma@rciqe.hokudai.ac.jp

Keywords:

A1. Nanowire, A1. Quantum well, A1. Photoluminescence,

A1. Transmission electron microscopy, A3. Metalorganic vapor phase epitaxy,

B2. AlGaAs/GaAs

PACS:

71.55.Eq,

61.46.Km,

81.10.Bk

Abstract

We developed a growth method for forming a GaAs quantum well contained in an AlGaAs/GaAs heterostructure nanowire by using selective-area metal organic vapor phase epitaxy. To find the optimum growth condition of AlGaAs nanowires, we changed the growth temperature between 800 and 850^{o}C and found that best uniformity of the shape and the size was obtained near 800^{o}C but lateral growth of AlGaAs became larger, which resulted in a wide GaAs quantum well grown on the top (111)B facet of the AlGaAs nanowire. To form the GaAs quantum well with a reduced lateral size atop the AlGaAs nanowire, a GaAs core nanowire about 100 nm in diameter was grown before the AlGaAs growth, which reduced the lateral size of AlGaAs to roughly half compared with that without the GaAs core. Photoluminescence measurement at 4.2 K indicated spectral peaks of the GaAs quantum wells about 60 meV higher than the acceptor-related recombination emission peak of GaAs near 1.5 eV. The photoluminescence peak energy showed a blue shift of about 15 meV, from 1.546 to 1.560 eV, as the growth time of the GaAs quantum well was decreased from 8 to 3 sec. Transmission electron microscopy and energy dispersive X-ray analysis of an AlGaAs/GaAs heterostructure nanowire indicated a GaAs quantum well with a

thickness of 5－20 nm buried along the <111> direction between the AlGaAs shells, showing a successful fabrication of the GaAs quantum well.

1. Introduction

Over the past several years, semiconductor nanowires (NWs) have attracted much attention because they might become an active element of next-generation integrated circuits and functional devices [1-3]. Field effect transistors [4], single electron transistors [5], light emitting devices [6-9], and chemical sensors [10, 11] using semiconductor NWs were fabricated to demonstrate their feasibilities and performances. These NW devices also are a focus of interest because they might allow us to explore new physics of nanostructures. To fabricate NW devices and extract the features and advantages over conventional devices, we have to grow NWs by precisely controlling the size and shape with high crystal quality.

Selective-area metal organic vapor phase epitaxy (SA-MOVPE) is a method for fabricating well-defined size- and position-controlled semiconductor NWs without using a growth catalyst [12-14]. The method eliminates concern over catalyst incorporation into grown crystals and thereby ensures high quality. By optimizing the growth condition of SA-MOVPE, we could obtain heterostructure NWs whose sizes were well controlled toward axial and radial directions [15]. We reported on the growth of GaAs/AlGaAs core-shell NWs [16] and an InGaAs quantum well (QW) embedded in

InGaAs/GaAs vertical heterostructure NWs [17, 18], which could be used as an active region of a light-emitting device operated at a 900-nm wavelength band. Another report by Heiβ et al., who focused on fabricating $In_xGa_{1-x}As$/GaAs vertical (axial) heterostructure NWs using catalyst-free growth during molecular beam epitaxy, indicated a possibility to control the crystal composition and thickness of the $In_xGa_{1-x}As$ segments as small as 100 nm [19]. Sköld et al. discussed the structure and optical properties of GaAs/InGaP core-shell NWs grown by the VLS method [20]. They found that the photoluminescence intensity of the GaAs core was increased by a few orders of magnitude compared with that without the InGaP shell.

AlGaAs/GaAs vertical heterostructure NWs are attractive for fabricating a NW light-emitting device at a wavelength of 850 nm. For the AlGaAs/GaAs heterojunction, we can ignore the effect of lattice mismatching between GaAs and AlGaAs on the change in the bandgap energy of a GaAs QW compared with that of GaAs/InGaAs or GaAs/InGaP lattice mismatched junctions. Therefore we could control the emission wavelength of the GaAs QW by changing the size of QW in the axial/lateral directions.

To date, the number of reports on AlGaAs/GaAs heterostructure NWs with a GaAs QW contained along the axial direction was limited [21-23], due mainly to difficulty in

controlling the size and the shape of AlGaAs. To fabricate a QW or a quantum dot (QD) buried along the axial direction of NW, we also need to control and optimize the growth condition.

We explain the experimental results of AlGaAs NW growth using SA-MOVPE to improve the uniformity of the diameter and height by reducing lateral (radial) growth. We then describe the formation of a GaAs QW buried in AlGaAs/GaAs heterostructure NWs and a grown structure which was characterized using scanning electron microscopy (SEM) and transmission electron microscopy (TEM) combined with energy dispersive X-ray analysis (EDX). We discuss the micro-photoluminescence (μ-PL) characteristics to confirm the formation of a GaAs QW in NWs and estimate the thickness of the QW.

2. Experimental procedure

The fabrication process of NWs, as shown in Fig. 1, began with the preparation of patterned GaAs(111)B substrates partially covered with a SiO_2 mask (thickness: 30 nm) for SA-MOVPE. The SiO_2 mask pattern was formed using electron beam (EB)

lithography and wet chemical etching and was designed to have a periodic array of SiO_2 window holes with a diameter, d_0, ranging from 80 to 110 nm and their periods, a, ranging from 0.5 to 3.0 μm. The periodic array had an area of 100 × 100 μm^2, which was separated from other periodic arrays with a 100-μm space. SA-MOVPE growth of undoped GaAs and AlGaAs was carried out in a horizontal reactor working at 0.1 atm.

The source materials used in the experiment were trimethylgallium (TMG), trimethylaluminum (TMA), and 20% arsine (AsH_3) in hydrogen. The formation of a NW sample with a GaAs QW buried in AlGaAs began with a GaAs core growth, followed by a growth sequence from an AlGaAs shell, a GaAs QW, an AlGaAs shell, and a GaAs cap layer. For the GaAs core and QW layer, the growth temperature was 750^oC, and the growth times were 5 min for the core and changed from 3 to 8 sec for QWs, respectively. The partial pressures for AsH_3 and TMG were 5.0×10^{-4} and 2.7×10^{-6} atm, respectively. For the AlGaAs shell, an optimum growth condition was chosen from preliminary experiments by changing the growth temperature between 800 and 850^oC and partial pressures of AsH_3 between 2.6×10^{-4} and 1.6×10^{-3} atm, TMG between 9.2×10^{-7} and 2.8×10^{-6} atm, and TMA between 1.6×10^{-7} and 4.8×10^{-7} atm. The optimum growth temperature and the growth time for the AlGaAs shell layer were

800^{o}C and 2.5 min, where the partial pressures for AsH_3, TMG, and TMA were 7.8 × 10^{-4}, 1.8 × 10^{-6}, and 3.2 × 10^{-7} atm, respectively. After the GaAs QW layer growth, an AlGaAs layer was grown under the same growth condition as those for the AlGaAs barrier-layer growth except that the growth temperature was changed beforehand from 750 to 800^{o}C, and the growth time was 20 sec.

3. Results and discussion

3.1 AlGaAs nanowire

We investigated how the shape of grown AlGaAs NWs changed with the growth temperature under a constant source pressure and a growth time of 20 min. Figures 2(a) to (c) show SEM images of AlGaAs NWs grown at 800, 825 and 850^{o}C, respectively. We found that NWs grown at 800^{o}C are uniform hexagonal structures and have crystal facets, which indicate formation of six (-110) equivalent side facets and the top (111)B facet. The diameter (d = 340 nm) of the NWs was larger than the mask-opening size (d_0 = 110 nm), which is due to the lateral growth of AlGaAs. The NW height decreased as the growth temperature increased from 800 to 850^{o}C, and the shape of crystals changed

from hexagonal to pyramid-like. The change in the crystal shape from hexagonal to pyramid-like as the growth temperature was increased is explained by the decrease of incorporation of source materials onto the (-110) equivalent side facets of hexagon. Ando et al. analyzed the crystal shape of GaAs and AlGaAs selectively grown within SiO_2 mask openings fabricated on a GaAs(111)B substrate [24]. According to their study, the grown shape of GaAs was a pyramid-like at temperatures higher than 750^{o}C but it became hexagonal below 750^{o}C under the constant source gas pressures. They discussed that the relative growth rate of GaAs between the (111)B and the (-110) planes was changed as the growth temperature or the source gas pressure was changed. The present result shown in Fig. 2 was focused on AlGaAs but the dependence of crystal shapes on the growth temperature was similar to that described by Ando et al.. We see on the SEM images in Fig. 2 that the volume of grown crystal was decreased as the temperature was increased. We think this was caused by the decrease in the incorporation rate of source materials onto the growth surface due to increased desorption/re-evaporation at higher temperatures. To form a GaAs QW on the (111)B facet of AlGaAs NWs and bury inside, we found the growth temperature of 800^{o}C was suitable.

Figure 3 shows the growth temperature dependence of the lateral growth thickness L_t and the uniformity of diameter for AlGaAs NWs. The thickness of lateral growth and the uniformity of diameter were characterized by measuring NW diameters on the SEM images. In Fig. 3, the error bar sizes for L_t look almost equal for the temperatures from 800 to 850^{o}C, but we consider here the uniformity of diameter in a relative way by using σ, the standard deviation of the NW diameter. The relative uniformity of diameter is defined as σ/d_{ave}, where d_{ave} is an average diameter of NWs. We can see from Fig. 3 that the lower the growth temperature, the better the relative uniformity and we obtained a best value of 7% at 800^{o}C. For the lateral growth, we could reduce L_t to about 30 nm at 850^{o}C from 90 nm at 800^{o}C, as shown in Fig. 3. We learned from this experiment that further optimization is necessary to satisfy both conditions at the same time to grow NWs with high uniformity and reduced lateral growth. It is thus important to clarify this mechanism.

Regarding the little difference in the size of the error bars for the lateral growth thickness L_t shown in Fig. 3, we think this was special to AlGaAs growth using SiO_2 mask openings and could be similar to the discussion of Ando et al. [25]. Based upon their argument, a relatively shorter diffusion length of Al atoms compared with Ga

atoms could decrease the diffusion of source materials onto the top of a NW. This, on the other hand, increases the lateral growth on the side facet. The higher lateral growth mode on the side (-110) facet of the AlGaAs NW could also be explained by a stronger bonding between Al and As atoms than that between Ga and As atoms in GaAs growth [25]. Another study describes that Al reacts with SiO_2 more than Ga does and the migration length of Al atoms (and growth species bonded with Al) was shorter than Ga [26]. Both reports state that the diffusion (migration) length becomes shorter as the temperature is lowered. We think this is why the lateral growth was increased as the growth temperature was decreased, as shown in Fig.3.

Ikejiri *et al.* reported on the suppression of lateral growth of GaAs NWs. They found a growth condition with a high growth temperature of up to 750^{o}C, and a low AsH_3 partial pressure was effective in reducing lateral growth compared with that at 600^{o}C and a relatively higher AsH_3 partial pressure [15]. For the AlGaAs NWs in the present study, the shape of grown AlGaAs was changed from hexagon pillar-like to tetrahedron-like when the growth temperature was increased from 800 to 850^{o}C. It is thus a challenge to reduce the lateral growth while maintaining a hexagon pillar shape.

3.2 AlGaAs/GaAs heterostructure nanowires and photoluminescence analysis

We explain the fabrication process of a GaAs QW buried in a heterostructure NW and PL analysis. To form a GaAs QW on top of an AlGaAs NW and confine carries in the QW three-dimensionally, the lateral growth of AlGaAs should be reduced. To achieve this, we introduced a GaAs core (height: about 600 nm, diameter: about 90 nm) growth before the first AlGaAs shell and then a GaAs QW was grown on top of the AlGaAs shell. We used a growth temperature of 800^{o}C to form the heterostructure based upon the relative uniformity of AlGaAs NWs discussed in Section 3.1.

To confirm whether the GaAs QW layer was grown on top of the (111)B facet or on the six (-110) side facets of the AlGaAs shell, a GaAs layer was grown after the formation of the GaAs/AlGaAs core-shell NW. Figures 4(a) to (c) show SEM images of GaAs NWs, GaAs/AlGaAs core-shell NWs (core-shell NWs), and GaAs/AlGaAs/GaAs heterostructure NWs (heterostructure NWs). Figure 4(d) shows the relationship of the height and diameter of NWs corresponding to the three growth steps shown in Figs. 4(a) to (c). Both the height and diameter of the NWs were increased during the growth steps from the GaAs NW to the core-shell NW. From the comparison of the core-shell NW with the heterostructure NW, the heterostructure NW was higher by 300 nm in average

than the core-shell NW, but the diameter was increased by about 10 nm, which indicates that the GaAs layer was grown dominantly on the top surface of the GaAs/AlGaAs core-shell NW. We think that once a very thin GaAs layer was deposited on the side (-110) facets of AlGaAs, the thin GaAs layer masked the active AlAs surface and the surface diffusion length of Ga atoms was increased to that of GaAs NW growth, as compared with AlGaAs NW growth discussed in section 3.1. Figures 4(e) to (h) show how the core-shell structure was effective to reduce the NW diameter compared with an AlGaAs/GaAs NW structure grown without the GaAs core. As seen in the SEM images of Figs. 4(g) and (h), we reduced the diameter of the GaAs top layer, by about 190 nm, to 150 nm. From the result, we could estimate the thickness of a GaAs layer deposited on the side facet of the GaAs/AlGaAs core-shell NW to be less than 0.3 nm when a GaAs QW as thin as 10－20 nm is grown on top of AlGaAs.

Figure 5(a) shows SEM images of heterostructure NWs with a GaAs QW buried in AlGaAs shells and a schematic cross-sectional structure (shown left). The height and diameter of NWs were about 1.2 μm and 180－260 nm. The diameter of the GaAs QW was assumed to be 140 nm for the structure, which was estimated from the change in NW diameters from the growth step of the core-shell NW to the heterostructure NW, as

shown in the SEM images and the plot of the NW diameter in Figs. 4(b), (c) and (d). We think the dispersion of the diameter for the core-shell NW (about ±15 nm (±11%)) should be projected on that of the GaAs QW.

The diameter of the AlGaAs outer shell was designed to be about 180 nm around the GaAs QW portion. Figure 5(b) shows the diameter distribution of the heterostructure NWs in Fig. 5(a). We found that the standard diameter deviation $\sigma_{diameter}$ of the NWs was about 29 nm, and the uniformity of diameter calculated using the ratio of $\sigma_{diameter}/d_{ave}$ was 14%. The apparent asymmetry of the histogram of NW diameter in Fig. 5(b) might be specific to the GaAs/AlGaAs heterostructure NWs containing a GaAs QW. When we grew AlGaAs NWs at 800°C (Fig. 3(a)), a histogram of the diameter indicated symmetry with $\sigma_{diameter}$ = 21 nm. For GaAs NWs, Motohisa et al. discussed that the histograms for the diameter indicated symmetry with $\sigma_{diameter}$ = 7－9 nm but the degree of the symmetry was slightly affected by the proximity effect of electron beam lithography when the pitch of SiO_2 mask openings was reduced from 0.6 μm to 0.4μm [27]. The standard deviation (σ) of NW diameters for the AlGaAs NWs or the GaAs/AlGaAs heterostructure NWs with a GaAs QW was roughly 2-4 times greater than that for the GaAs NWs. We think the increase in the diameter dispersion might be

attributed to AlGaAs growth.

We measured the μ-PL of the heterostructure NWs at 4.2 K. In this experiment, a He－Ne laser (wavelength: λ = 632.8 nm) was used as an excitation source with a maximum excitation power of about 1 kW/cm^2 and was focused on about a 2-μm diameter on the sample surface. Figure 6 shows the PL spectra of the three types of heterostructure NWs with a GaAs QW grown for the growth times of 3, 5 and 8 sec. For reference, a PL spectrum of GaAs NWs is also plotted. The number of NWs excited by the laser beam was about 3－5 for the samples with a NW pitch of 1 μm. The PL spectra for the three types of heterostructure NWs show strong emission peaks near a photon energy of 1.5 eV, which might have originated from the carbon acceptor-related recombination emission. The PL spectrum of GaAs NWs also shows a main peak near 1.49－1.50 eV, which is about 20 meV below the second main peak at 1.515 eV, corresponding to the band-to-band recombination emission. We can see a weak peak at 1.546 eV for the heterostructure NW with a GaAs QW grown at 8 sec. The peak energy shifted to 1.560 eV for the sample with a GaAs QW grown at 3 sec. Noborisaka *et al.* reported that the PL intensity of GaAs NWs was an order of magnitude weaker than that of GaAs/AlGaAs core-shell NWs [16]. Our results coincided well with their measurements,

and we confirmed that the AlGaAs shell worked as a passivation of the GaAs core NW. For the PL intensity of the GaAs QW, it was one order of magnitude weaker than that of the acceptor-related emission, as shown in Fig. 6. We believe this was caused by two factors. The first factor was that the volume of the GaAs QW was about 1/30 of the GaAs core. The second factor was that the Al composition of the AlGaAs NW measured using PL measurements was about 0.11, which was roughly equal to that of the outer shell measured using EDX. The difference in the energy bandgap between the GaAs QW and the AlGaAs shell is thus estimated as low as 0.11 eV, which is not sufficient to confine photo-excited carriers in the conduction band of the GaAs QW, compared with a GaAs QW sandwiched by AlAs barriers [28].

Figure 7(a) plots the GaAs QW width (thickness along the <111> direction) estimated from the PL peak energy versus that calculated by the GaAs NW growth rate along the <111> direction. The insert in Fig. 7(a) shows a dark-filed scanning TEM (STEM) image of the top region of a heterostructure NW with a GaAs QW for a growth time of 5 sec. A depth profile for Al composition measured using EDX is plotted on the left side of the STEM image in Fig. 7(a). The Al composition profile indicates different peak values above or below the GaAs QW. This might have been attributed to

different growth temperatures for the AlGaAs shells, but the reason is not clear. Figures 7(b) and (c) show a bright-field STEM image and a transmission electron diffraction pattern for the heterostructure NW portion from the GaAs QW region to the NW top. A high-resolution TEM image of the NW top center is shown in Fig. 7(d). A dark-field STEM image corresponding to the top half of that in Fig. 7 (a) is shown in Fig. 7(e). We found that the heterostructure NW with a GaAs QW had stacking faults perpendicular to the <111> direction, which are distributed along the <111> with a frequency ranging from a few nm to 20 nm as seen in Fig. 7(b). The crystal structure was found to be zincblende with rotational twins around the <111> axis (Fig. 7(c)). The stacking faults are originated from the rotational twins, which are confirmed by a high-resolution TEM image taken near the top surface of the NW, as shown in Fig. 7 (d). In Fig. 7 (e), the positions for the GaAs QW and the AlGaAs barriers are indicated with broken arrow lines, which are spotted by the light-and-dark contrast on the STEM image except for the fine ones caused by the stacking faults. We find on the STEM images in Figs. 7(b) and (e) that some of the stacking faults are distributed in the GaAs QW region.

To obtain the QW width from the PL measurements, we used formulas for the optical transition between the energy levels of electrons and holes, which are described as

follows [29, 30].

$$\hbar\omega = E_g(GaAs) + E_1 + E_{hh1}\,, \qquad (1)$$

and the quantized energy level E for electrons or holes with an effective mass m is given by

$$E = \left(\hbar^2\pi^2/2m\right)\left(n/L_{QW}\right)^2, \qquad (2)$$

where $\hbar = h/2\pi$ (h: Planck's constant), ω is an angular frequency of light, $E_g(GaAs)$ is the GaAs bandgap, n is a positive integer, E_1 is the lowest energy level of electrons in the conduction band, E_{hh1} is the lowest energy level of heavy holes in the valence band, and L_{QW} is the width of GaAs QW along the axial direction of the NW. The effective masses for the electrons and heavy holes used for the fitting were $m_e^* = 0.067$, $m_{hh}^* = 0.45$, respectively [29, 30]. We assumed the energy barrier height was infinite and the quantum confinement was only in the <111> direction and ignored the lateral confinement perpendicular to the <111> direction, for simplicity. The depth profile of the Al composition shown in the insert in Fig. 7(a) indicates that a GaAs QW with a thickness of 5－20 nm was formed about 150 nm from the top surface of the heterostructure NW. For the dark-field STEM image in Fig. 7(e), the GaAs/AlGaAs

heterojunction interface looks diffuse, but we estimate the thickness of the GaAs QW along the <111> is roughly 30 nm, which is greater than that obtained by EDX. We cannot find the GaAs/AlGaAs core-shell interface along the lateral direction of the GaAs QW on the dark-field STEM image, because we can hardly see light-and-dark contrast laterally. Tambe et al. discussed the heterojunction interface structure of a GaAs/$Al_xGa_{1-x}As$ core-shell NW from the images of dark-field STEM. They used an Al composition $x = 0.9$ for the sample and a high contrast at the interface was obtained [31]. We think the difference in the GaAs QW thickness measured by EDX and that by the STEM image is caused by low Al content in the AlGaAs barriers compared with that Tambe reported. The GaAs QW thickness measured using EDX is rather in fair agreement with that estimated with the PL spectra or the GaAs NW growth rate. These results indicate a successful fabrication of the GaAs QW using SA-MOVPE.

Figure 8 shows the PL spectra for heterostructure NWs with a GaAs QW grown with a different NW pitch from 0.5 to 3.0 μm. The growth time of the GaAs QW was 5 sec. We found a broad weak peak of the GaAs QW at the 50－70 meV higher energy side of a strong emission peak near 1.5 eV, corresponding to the acceptor-related recombination emission. The broad weak peak position shifted to a higher energy region from 1.548 to

1.567 eV as the NW pitch increased from 0.5 to 3.0 μm. We found the PL intensity became weak as the NW pitch changed from 0.5 to 3 μm. This was caused by the decrease in the number of NWs excited by the laser beam as the pitch increased. The insert graph in the upper right of Fig. 8 shows that the GaAs QW width estimated from the PL peak energy decreases as the NW pitch increases. This means the GaAs growth rate along the <111>B direction decreased on top of AlGaAs as the NW pitch increased, which is further evidence of the growth rate dependence of GaAs NWs on the NW pitch discussed by Noborisaka *et al.* [13]. Regarding the broad PL peaks of the GaAs QW compared with the relatively sharp acceptor-related emission peaks of the GaAs core, a broad distribution of the GaAs QW thickness along the <111> direction might be a cause. We found that there was a distribution of the NW height, as can be seen from the SEM image in Fig. 5(a). The change in the NW height implies a distribution of the GaAs QW thickness buried inside, which means spectral broadening of PL.

4. Conclusion

We grew AlGaAs/GaAs heterostructure NWs with a GaAs QW buried inside by

using SA-MOVPE. We found that the introduction of a GaAs core NW was effective in reducing the lateral growth of an AlGaAs shell and in forming a GaAs QW with a reduced diameter between the AlGaAs shells. TEM-EDX analysis indicated that a GaAs QW as thin as 5－20 nm was grown, whose thickness was roughly equal to that estimated with spectral peak energy of photoluminescence. We believe our method for fabricating a GaAs QW buried between the AlGaAs shells will be useful for the formation of semiconductor NW devices with QWs buried along the axial direction of the NW.

Acknowledgments

The authors would like to thank Dr. Kumar S. K. Varadwaj for supporting PL measurements. We also wish to acknowledge H. Yoshida and T. Wakatsuki for their support in the MOVPE experiment. This work was financially supported by a grant-in-aid for Scientific Research from the MEXT in Japan.

References

[1] Y. Cui, Z. Zhong, D. Wang, W. U. Wang, and C. M. Lieber, *Nano Lett.* **3** (2003) 149.

[2] M. T. Björk, O. Hayden, H. Schmid, H. Riel, and W. Riess, *Appl. Phys. Lett.* **90** (2007) 142110.

[3] T. Bryllert, L.-E. Wernersson, T. Löwgren, and L. Samuelson, *Nanotechnology* **17** (2006) S227.

[4] T. Tanaka, K. Tomioka, S. Hara, J. Motohisa, E. Sano, and T. Fukui, *Appl. Phys. Express* **3** (2010) 025003.

[5] A. Fuhrer, L. E. Fröberg, J. N. Pedersen, M. W. Larsson, A. Wacker, M.-E. Pistol, and L. Samuelson, *Nano Lett.* 7 (2007) 243.

[6] K. Hiruma, M. Yazawa, T. Katsuyama, K. Ogawa, K. Haraguchi, M. Koguchi, and H. Kakibayashi, *J. Appl. Phys.* **77** (1995) 447.

[7] F. Qian, Y. Li, S. Gradečak, D. Wang, C. J. Barrelet, and C. M. Lieber, *Nano Lett.* **4** (2004) 1975.

[8] B. Hua, J. Motohisa, Y. Kobayashi, S. Hara, and T. Fukui, *Nano Lett.* **9** (2009) 112.

[9] L. K. v. Vugt, S. Rühle, and D. Vanmaekelbergh, *Nano Lett.* **6** (2006) 2707.

[10] C. Li, D. Zhang, X. Liu, S. Han, T. Tang, J. Han, and C. Zhou, *Appl. Phys. Lett.* **82** (2003) 1613.

[11] Z. Fan, D. Wang, P.-C. Chang, W.-Y. Tseng, and J. G. Lu, *Appl. Phys. Lett.* **85** (2004) 5923.

[12] T. Hamano, H. Hirayama, and Y. Aoyagi, *Jpn. J. Appl. Phys.* **36** (1997) L286.

[13] J. Noborisaka, J. Motohisa, and T. Fukui, *Appl. Phys. Lett.* **86** (2005) 213102.

[14] K. Sladek, V. Klinger, J. Wensorra, M. Akabori, H. Hardtdegen, and D. Grützmacher, *J. Cryst. Growth* **312** (2010) 635.

[15] K. Ikejiri, J. Noborisaka, S. Hara, J. Motohisa, and T. Fukui, *J. Cryst. Growth* **298** (2007) 616.

[16] J. Noborisaka, J. Motohisa, S. Hara, and T. Fukui, *Appl. Phys. Lett.* **87** (2005) 093109.

[17] L. Yang, J. Motohisa, J. Takeda, K. Tomioka, and T. Fukui, *Appl. Phys. Lett.* **89** (2006) 203110.

[18] L. Yang, J. Motohisa, J. Takeda, K. Tomioka, and T. Fukui, *Nanotechnology* **18** (2007) 105302.

[19] M. Heiβ, A. Gustafsson, S. C-Boj, F. Peiró, J. R. Morante, G. Abstreiter, J. Arbiol, L. Samuelson, and A. F. i Morral, *Nanotechnology* **20** (2009) 075603.

[20] N. Sköld, L. S. Karlsson, M. W. Larsson, M.-E. Pistol, W. Seifert, J. Trägårdh, and L. Samuelson, *Nano Lett.* **5** (2005) 1943.

[21] K. Ishikawa, N. Yamamoto, K. Tateno, and Y. Watanabe, *Jpn. J. Appl. Phys.* **47** (2008) 6596.

[22] C. Chen, N. Braidy, C. Couteau, C. Fradin, G. Weihs, and R. Lapierre, *Nano Lett.* **8** (2008) 495.

[23] J. Heinrich, A. Huggenberger, T. Heindel, S. Reitzenstein, S. Höfling, L. Worschech, and A. Forchel, *Appl. Phys. Lett.* **96** (2010) 211117.

[24] S. Ando, N. Kobayashi, and H. Ando, *J. Cryst. Growth* **145** (1994) 302.

[25] S. Ando, and T. Fukui, *J. Cryst. Growth* **98** (1989) 646.

[26] K. Hiruma, T. Haga, and M. Miyazaki, *J. Cryst. Growth* **102** (1990) 717.

[27] J. Motohisa, J. Takeda, M. Inari, J. Noborisaka, and T. Fukui, *Physica E* **23** (2004) 298.

[28] M. Nakayama, T. Hirao, and T. Hasegawa, *J. Appl. Phys.* **105** (2009) 123525.

[29] S. M. Sze, *Physics of Semiconductor Devices*, 2nd edition, John Wiley & Sons, New York, 1981, p. 730

[30] R. Dingle, W. Wiegmann, and C. H. Henry, *Phys. Rev. Lett.* **33** (1974) 827.

[31] M. J. Tambe, L. F. Allard, and S. Gradecak, *J. Phys.*: Conf. Ser. **209** (2010) 012033.

Figure captions

Fig. 1. Schematic fabrication procedure for NWs

Fig. 2. SEM images of AlGaAs NWs for growth time of 20 min. Growth temperatures are 800, 825 and 850^{o}C for (a)-(c), respectively. NW pitch a = 0.5 μm.

Fig. 3. Growth temperature dependence of lateral growth thickness L_t and relative uniformity of diameter for AlGaAs NWs

Fig. 4. SEM images of NWs and changes in NW height and diameter. NW pitch a = 1.0 μm and SiO_2 mask opening size d_0 = 80 nm. (a), (b) and (c) are SEM images for GaAs NWs, core-shell NWs, and heterostructure NWs, respectively. White dotted parallel lines bridged between SEM images (a) and (b), or (b) and (c) indicate how the NW height changed between the growth steps, for clarity. (d) Changes in height and diameter of NWs corresponding to growth steps of GaAs NW (GaAs core growth time: 5.0 min), GaAs/AlGaAs core-shell NW (AlGaAs shell growth time: 2.5 min), and GaAs/AlGaAs/GaAs heterostructure NW (top GaAs growth time: 2.0 min). (e) and (f) illustrate reduction in NW diameter by introduction of GaAs core. (g) and (h) show SEM images of NW grown with and without GaAs core, corresponding to the

schematics of (e) and (f), respectively. For the structure shown in (f) and (h), the growth times of AlGaAs and GaAs are 20.0 and 5.0 min, respectively.

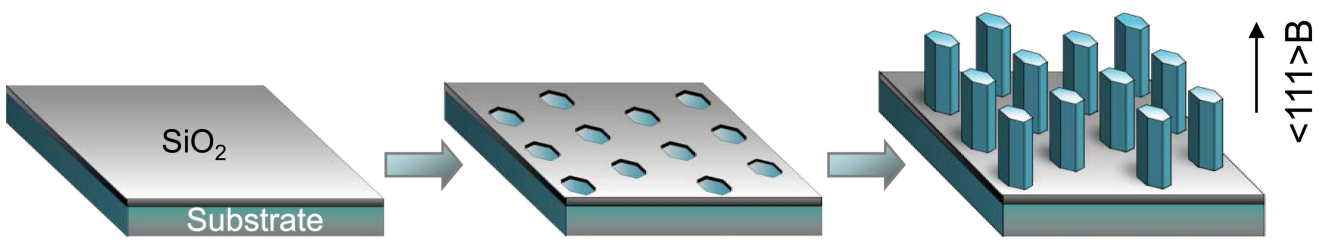
Fig. 5. SEM images and schematic structure of heterostructure NWs and distribution of diameter. (a) SEM images of grown NWs and schematic cross-sectional structure of NW containing GaAs QW. A GaAs cap layer is not shown in the schematic. Insert SEM image in upper right shows top view of NW. (b) Histogram of diameter distribution for NWs with pitch a = 0.5 μm.

Fig. 6. PL spectra for heterostructure NWs and GaAs NWs measured at 4.2 K. NW pitch was 1 μm.

Fig. 7. GaAs QW width calculated by PL spectra and growth rate and analysis by TEM. (a) Comparison of GaAs QW width obtained by PL peak energy with that estimated by axial growth rate of GaAs NW. NW pitch was 1 μm. Insert in upper right shows dark-field STEM image of heterostructure NW taken with electron beam direction parallel to <-110>. Insert left above shows depth profile of Al composition measured from top of NW by EDX, which indicates GaAs QW portion sandwiched by AlGaAs. A white broken line along <111> direction on the STEM image shows the path scanned by

electron beam for EDX. (b) Bright-field STEM image of NW. (c) Transmission electron diffraction pattern. (d) High-resolution TEM image of a NW top portion indicated with white rectangle on the STEM image of (b). Twin boundaries are indicated with arrows. (e) Dark-field STEM image of (b). Layer positions of GaAs QW and AlGaAs barriers estimated along the <111> direction are indicated with broken arrow lines.

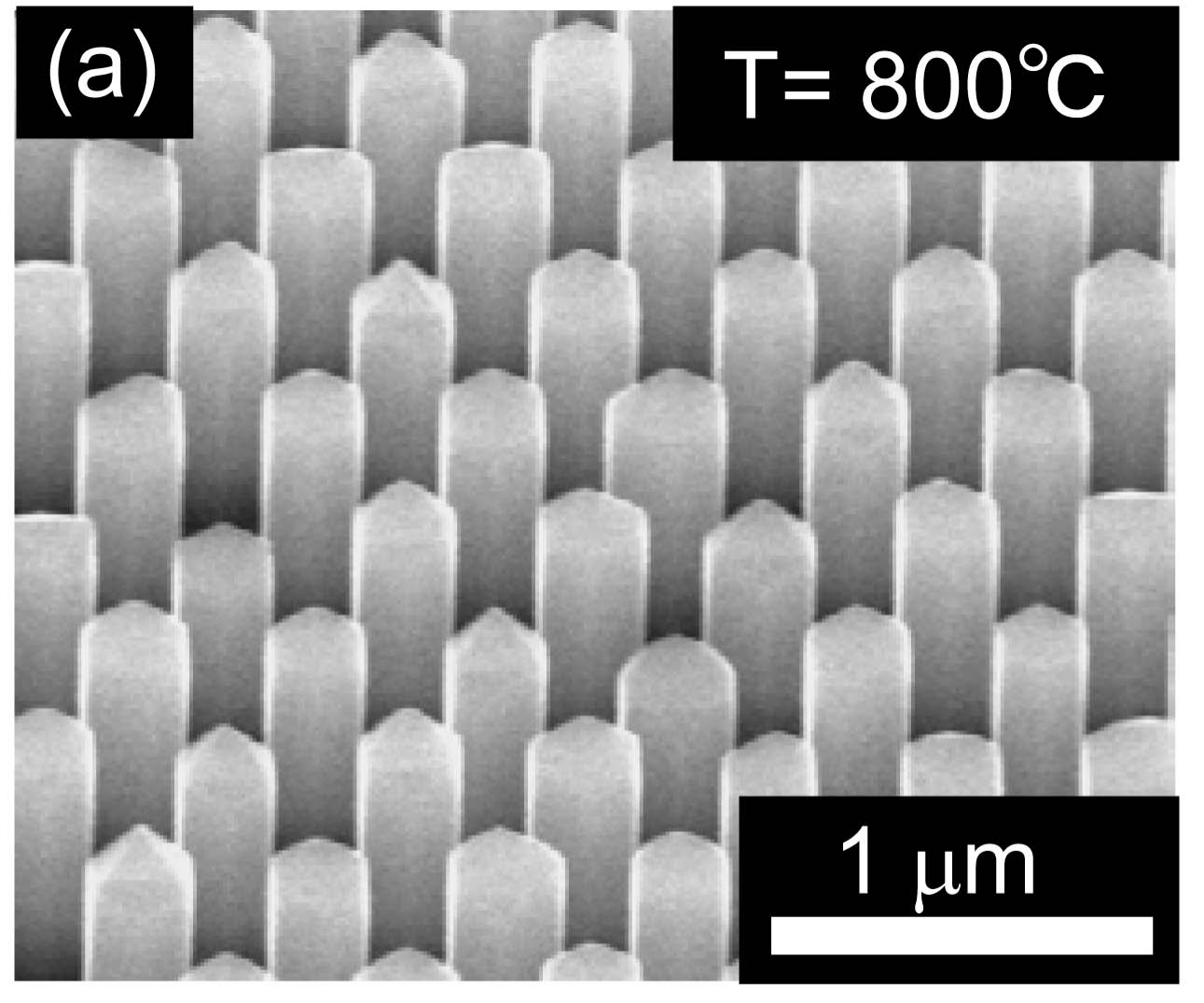
Fig. 8. NW pitch dependence of PL spectra for heterostructure NWs containing GaAs QW. Insert graph shows GaAs QW width as function of NW pitch

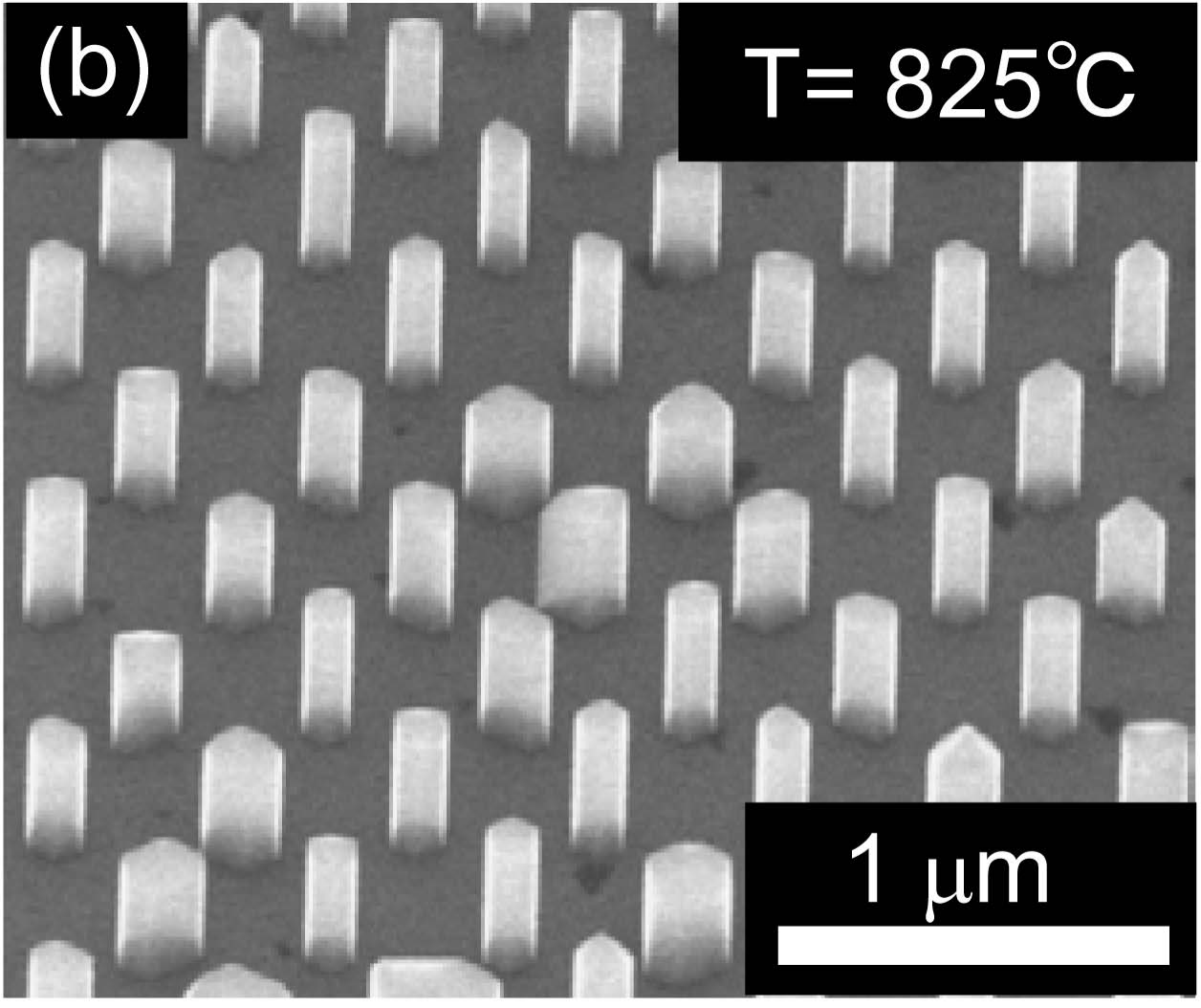


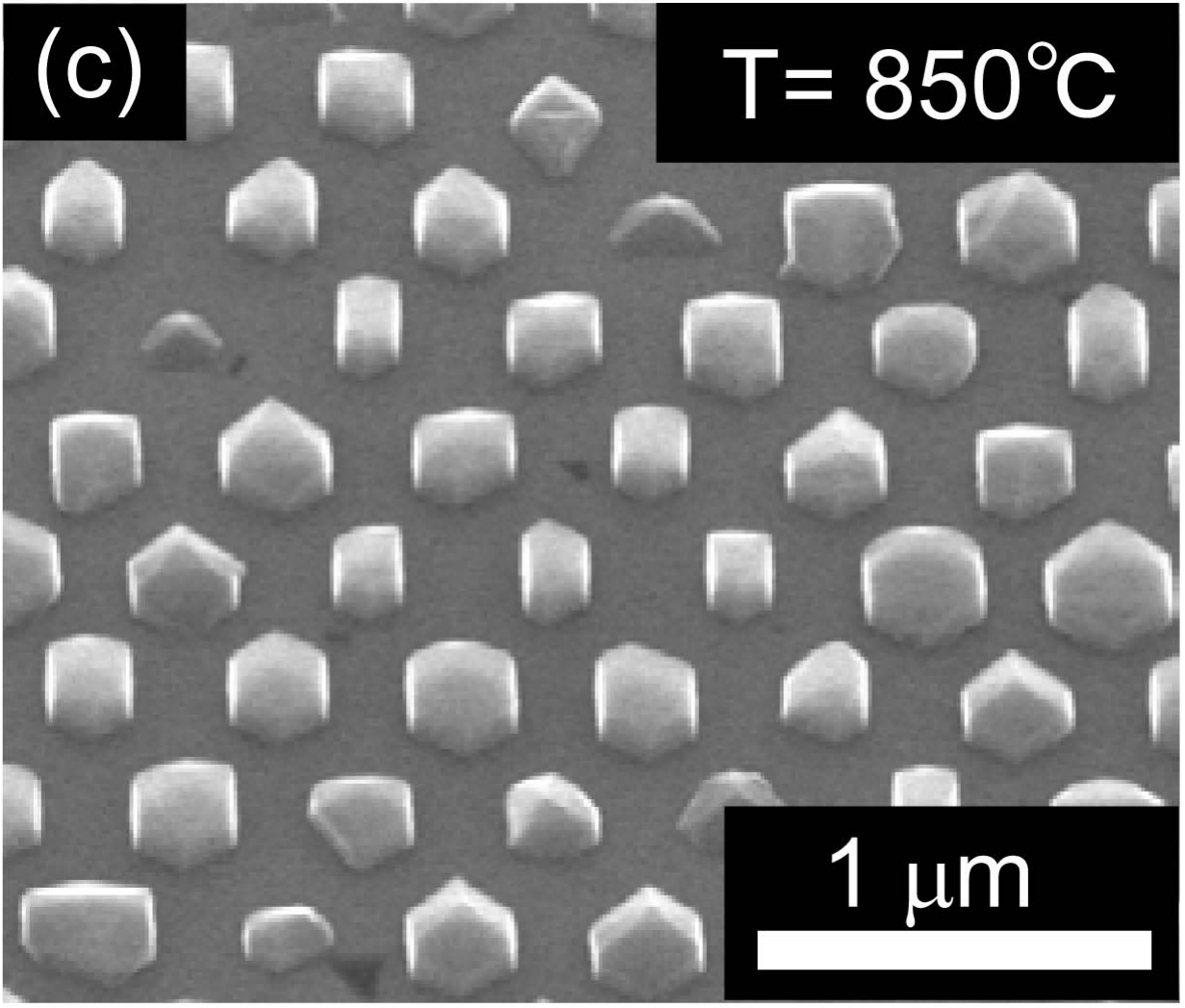
Deposition of SiO_2 film

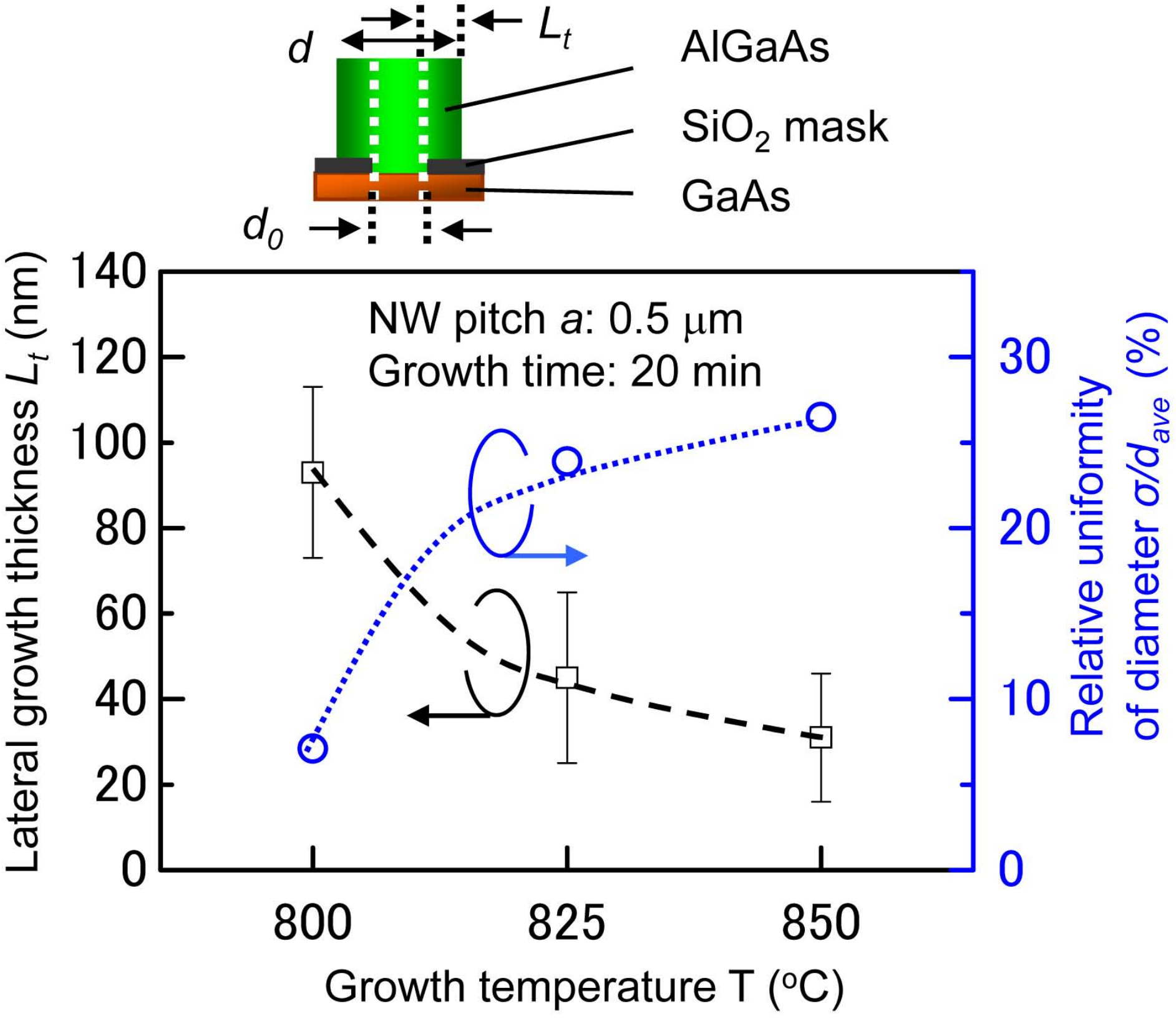
Mask fabrication by EB lithography and wet etching

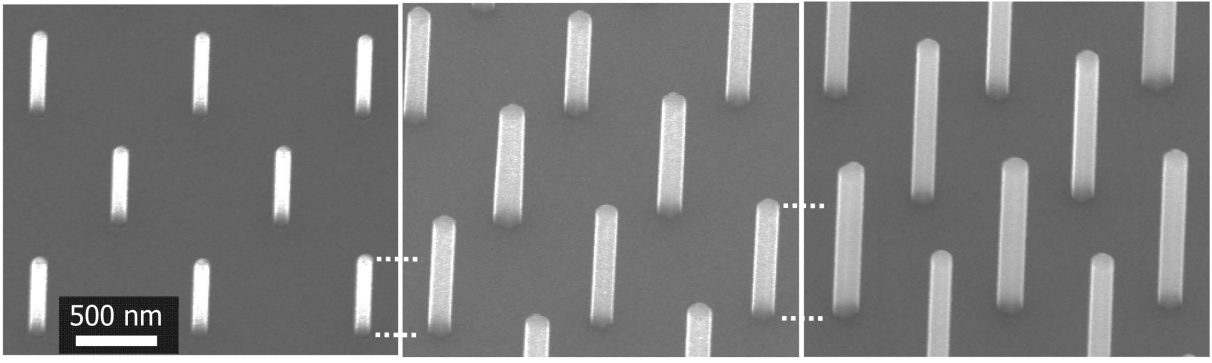
MOVPE growth

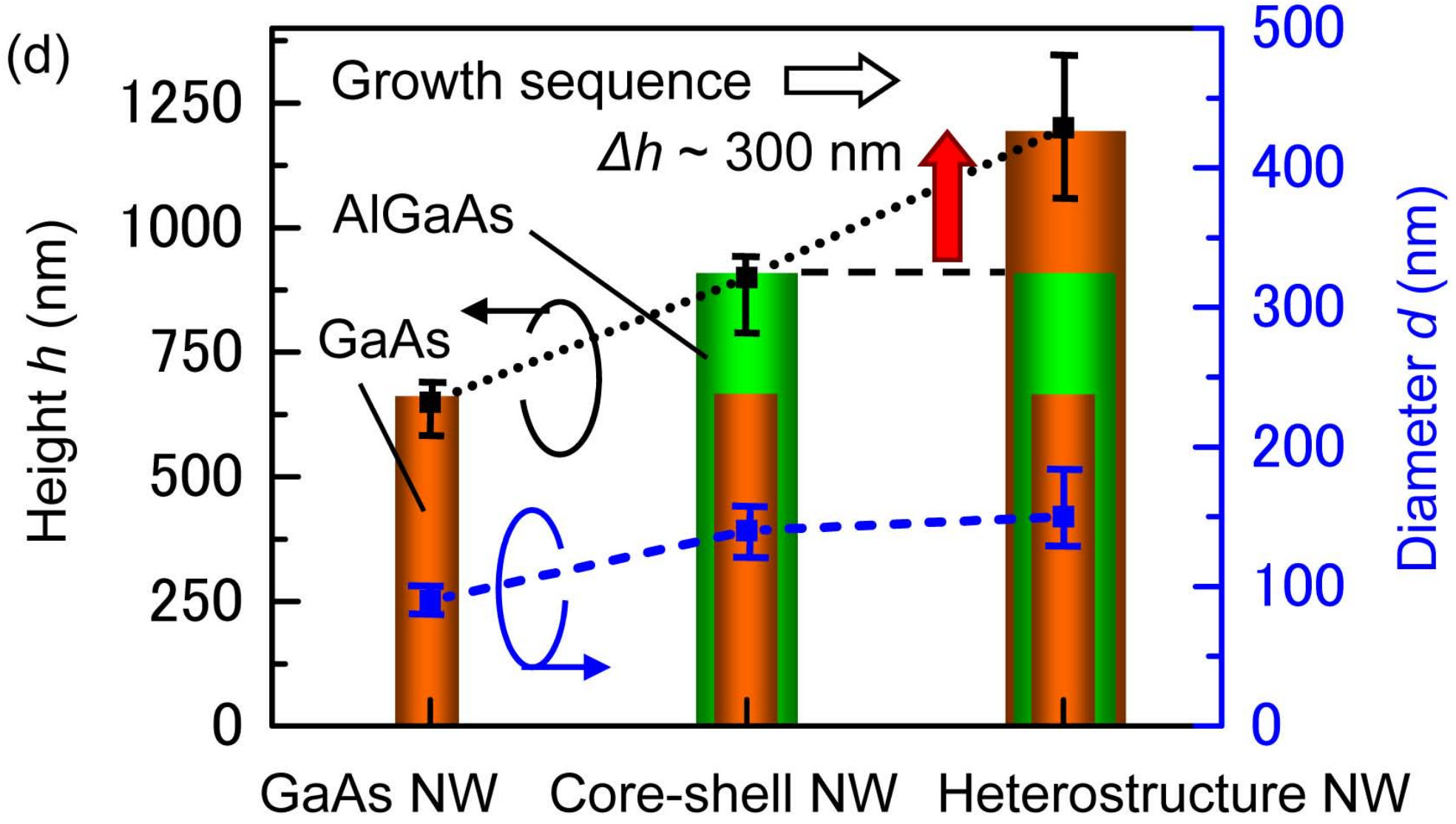

(a)
T= 800℃
1 μm

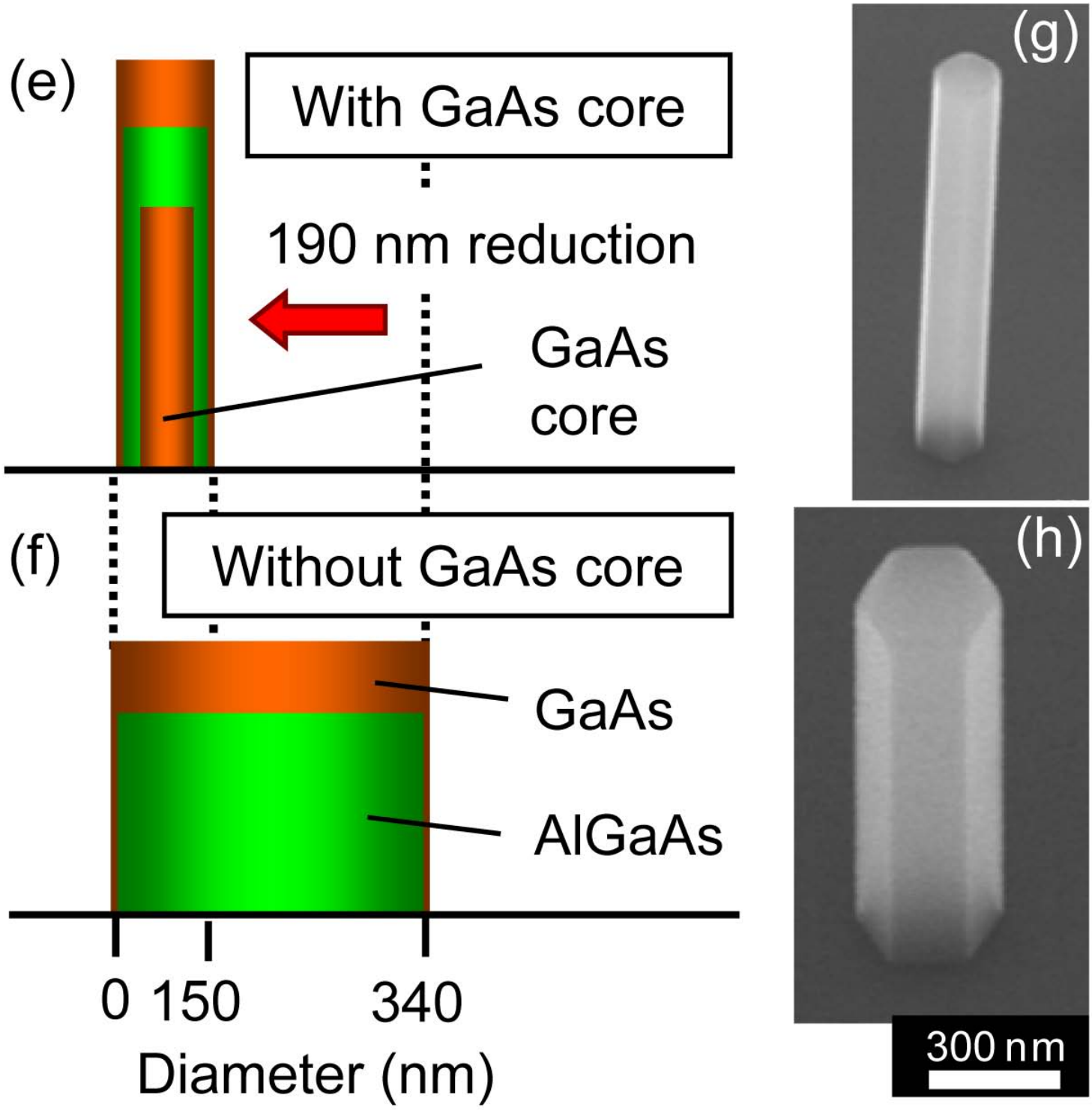

(b)
T= 825℃
1 μm

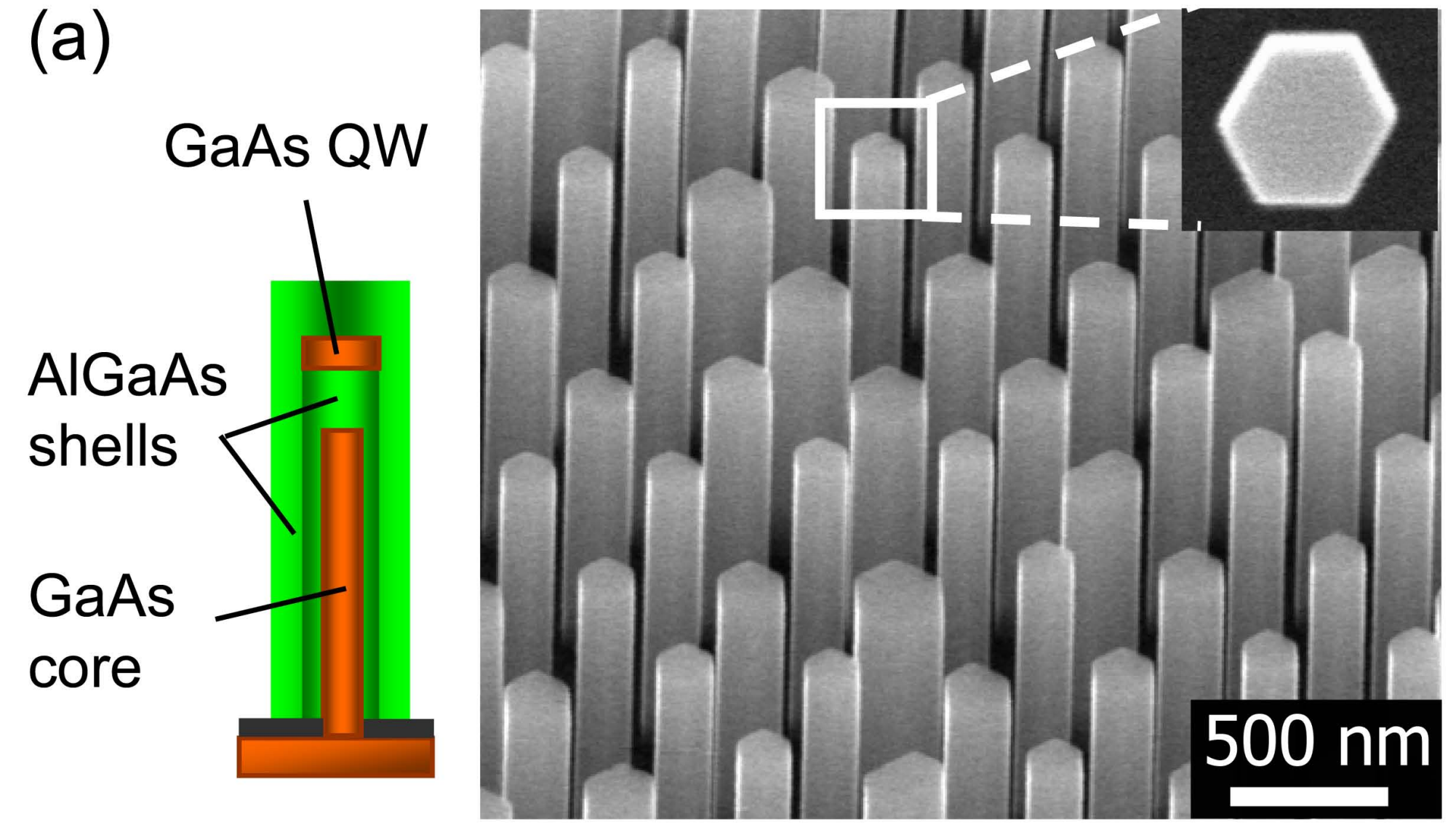

(c)
T= 850℃
1 μm

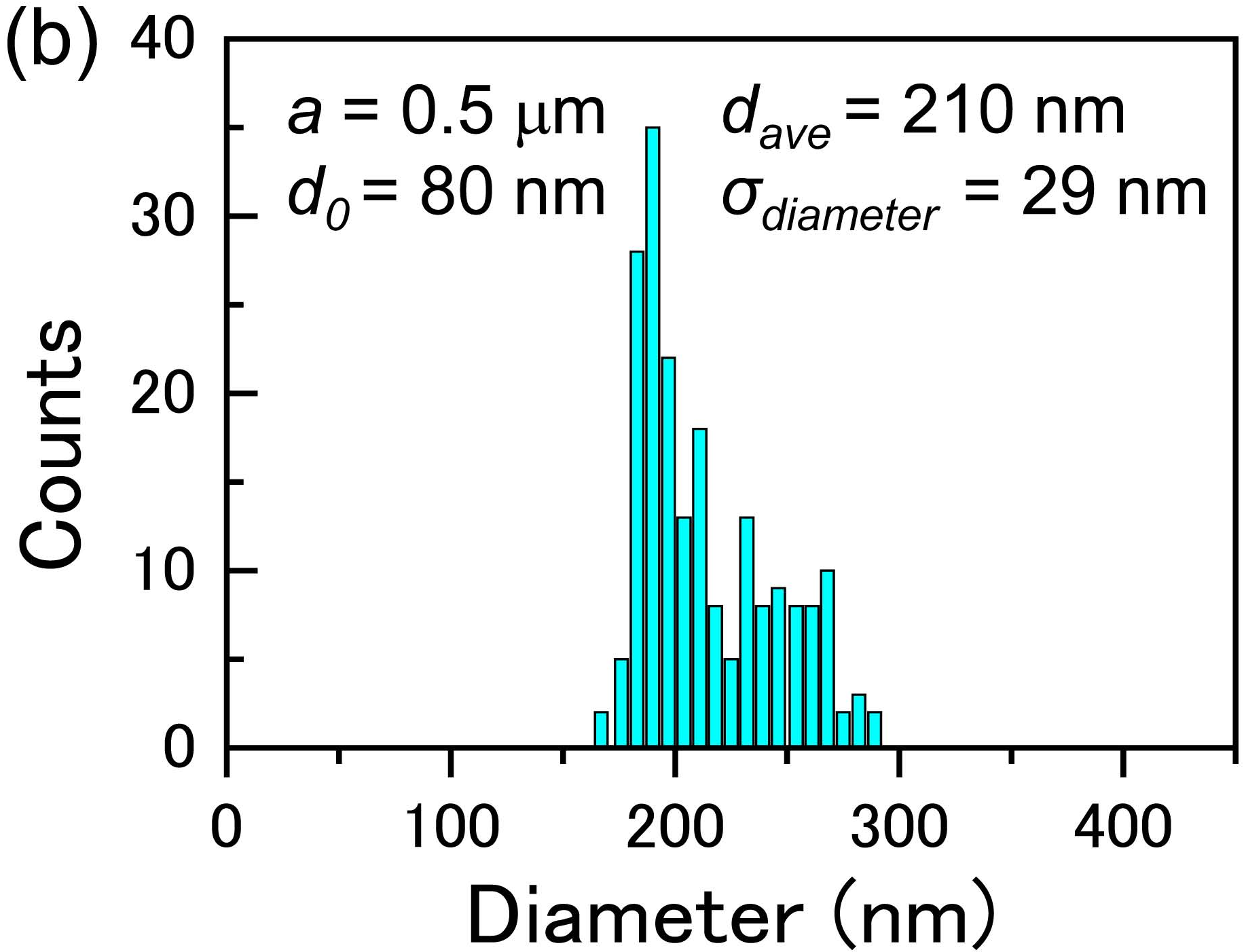

d
L_t
AlGaAs
SiO_2 mask
GaAs
d_0
NW pitch a: 0.5 μm
Growth time: 20 min
Lateral growth thickness L_t (nm)
Relative uniformity of diameter σ/d_{ave} (%)
Growth temperature T (°C)
0
20
40
60
80
100
120
140
0
10
20
30
800
825
850

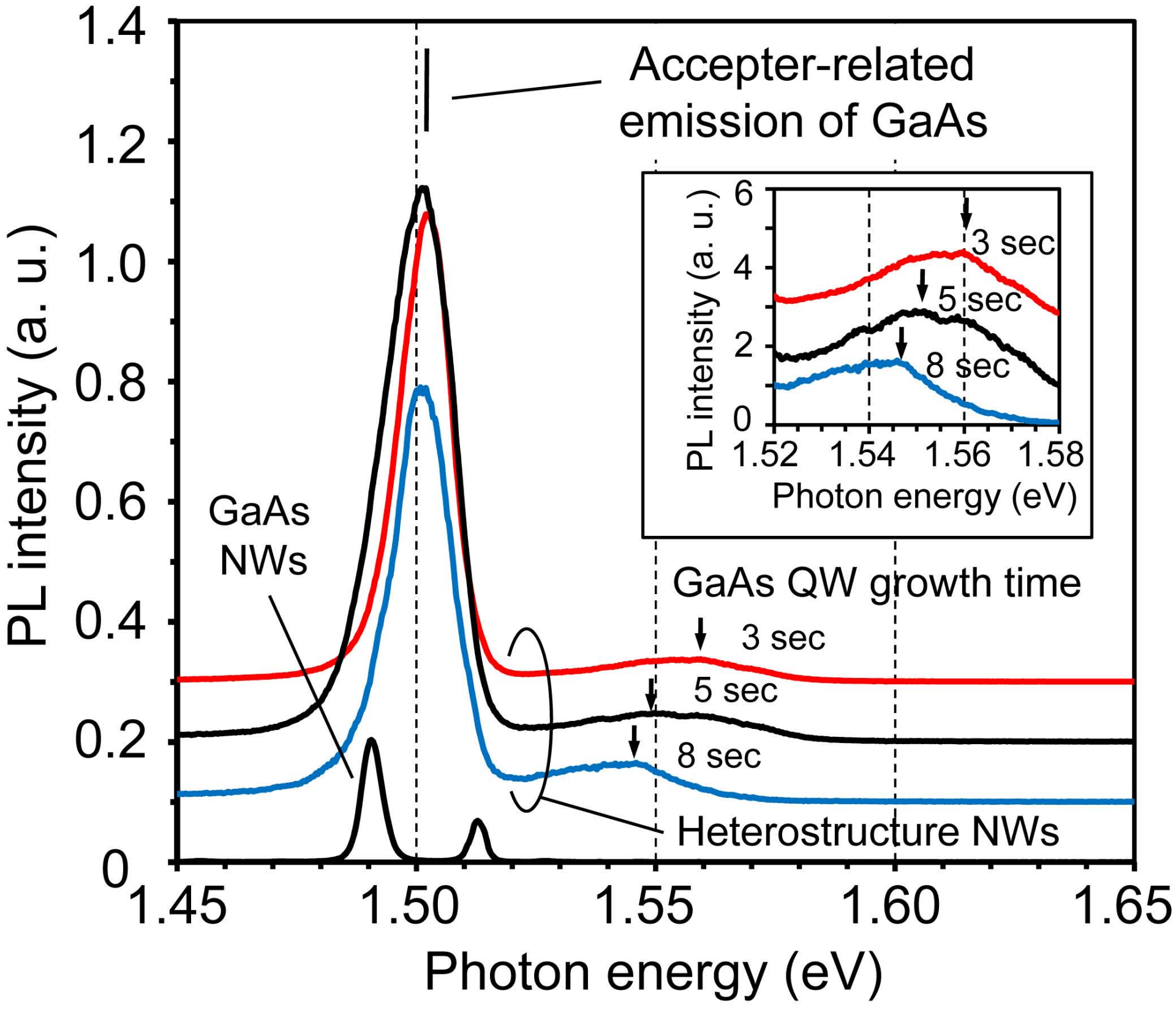

(a) GaAs NWs
(b) Core-shell NWs
(c) Heterostructure NWs
500 nm
d_{ave} = 90 nm
d_{ave} = 140 nm
d_{ave} = 150 nm

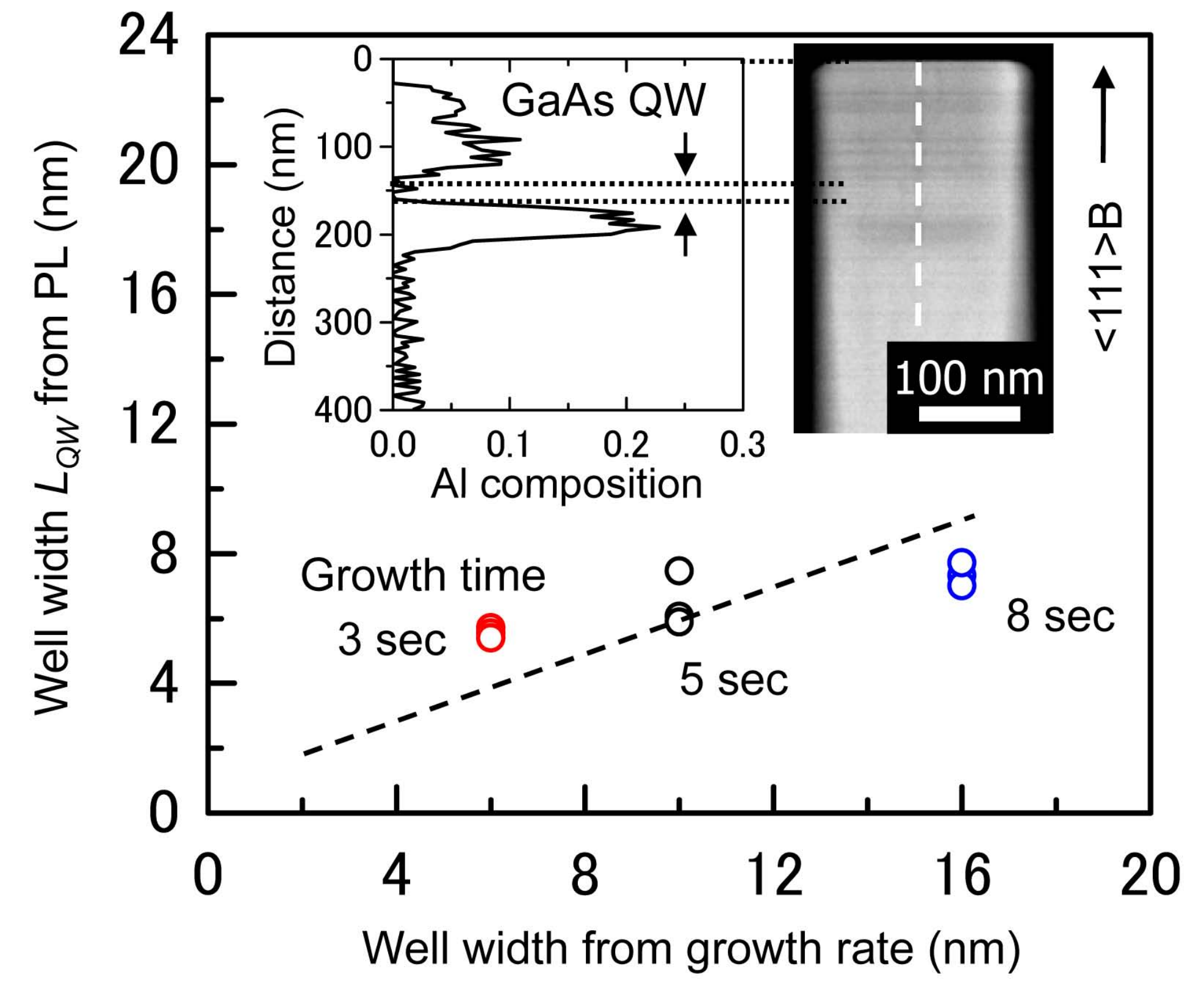

(d)
Growth sequence
Δh ~ 300 nm
AlGaAs
GaAs
Height h (nm)
Diameter d (nm)
1250
1000
750
500
250
0
500
400
300
200
100
0
GaAs NW
Core-shell NW
Heterostructure NW

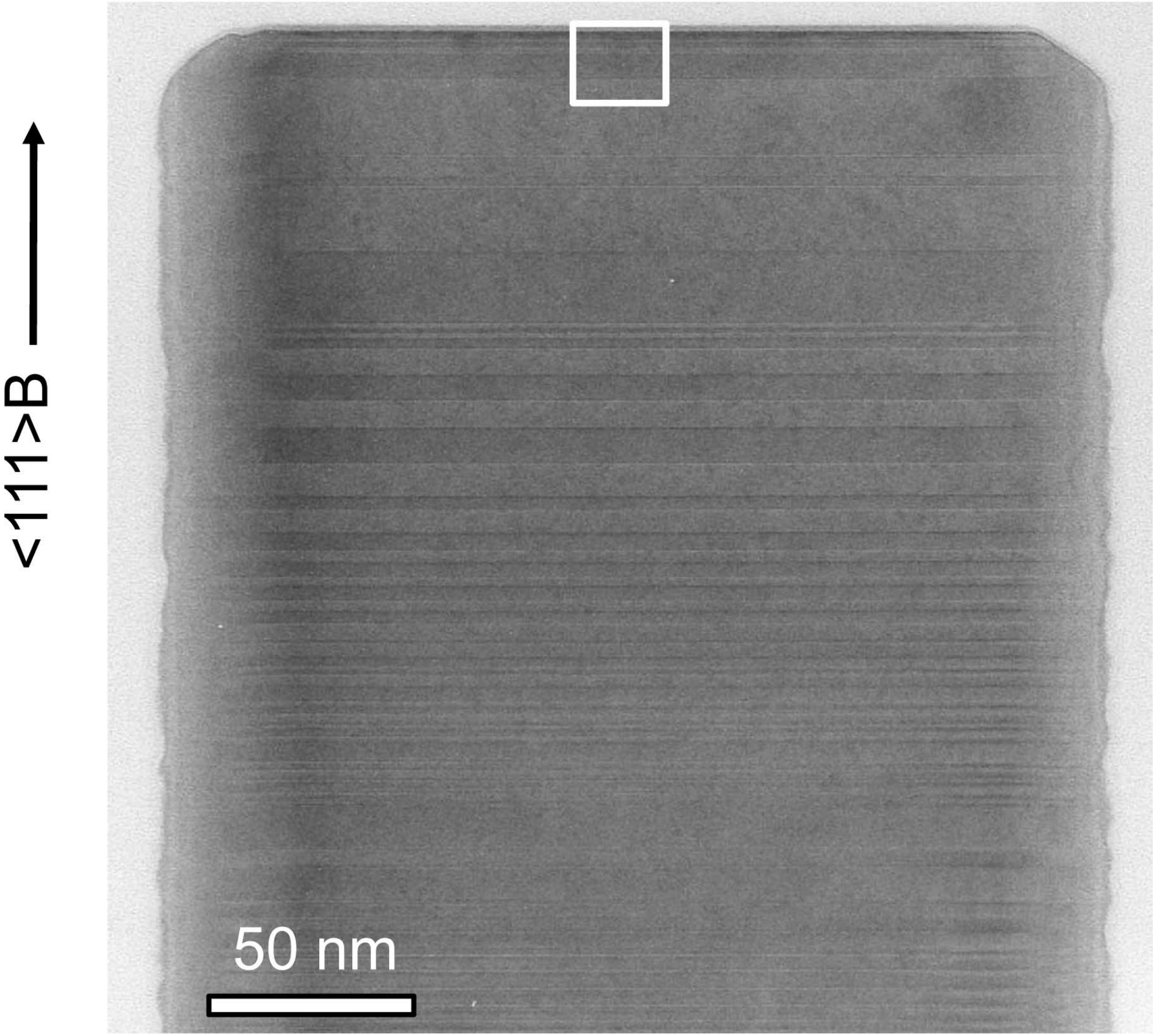

(e)
With GaAs core
190 nm reduction
GaAs
core
(f)
Without GaAs core
GaAs
AlGaAs
0
150
340
Diameter (nm)
(g)
(h)
300 nm

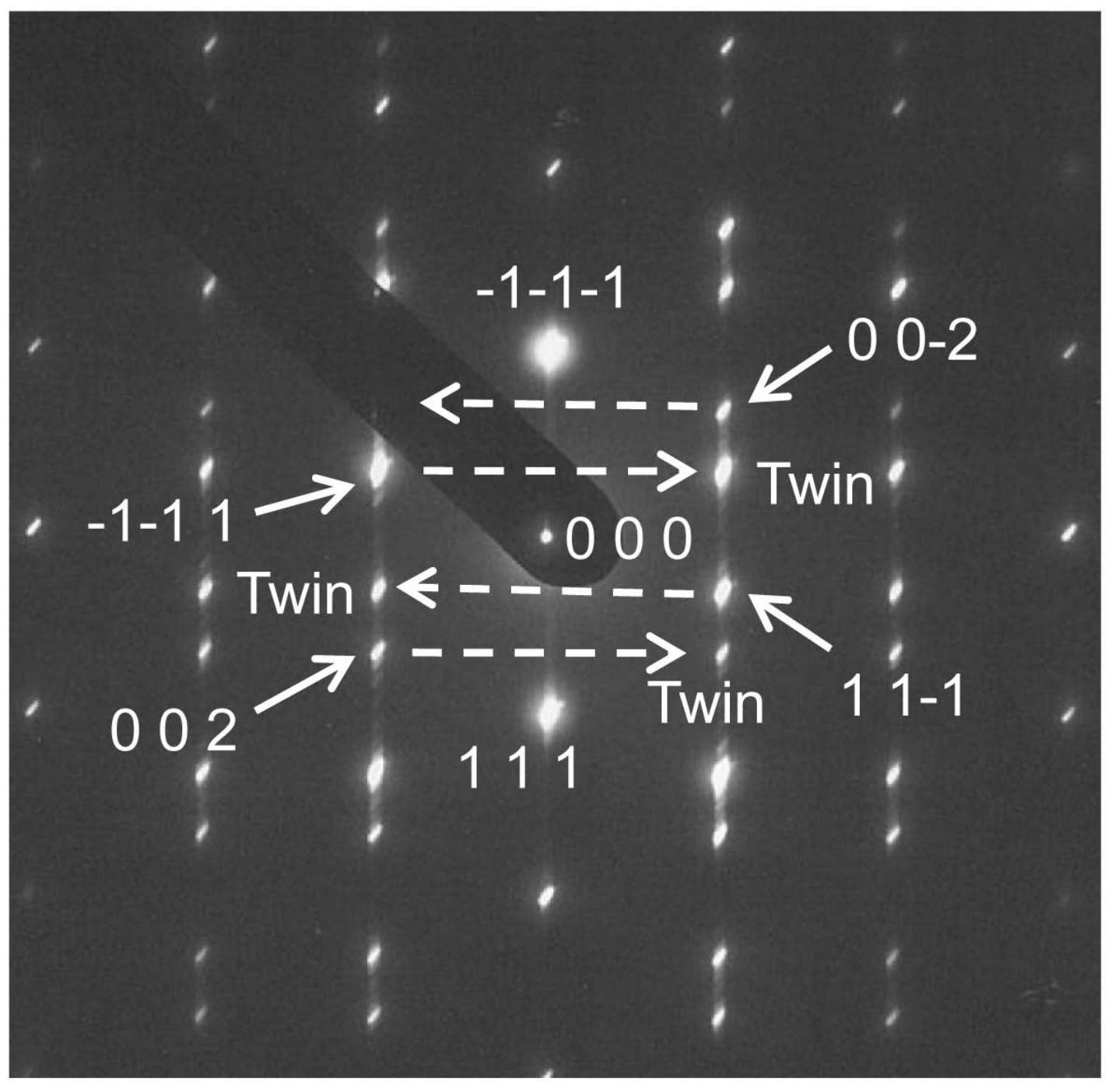

(a)
GaAs QW
AlGaAs
shells
GaAs
core
500 nm

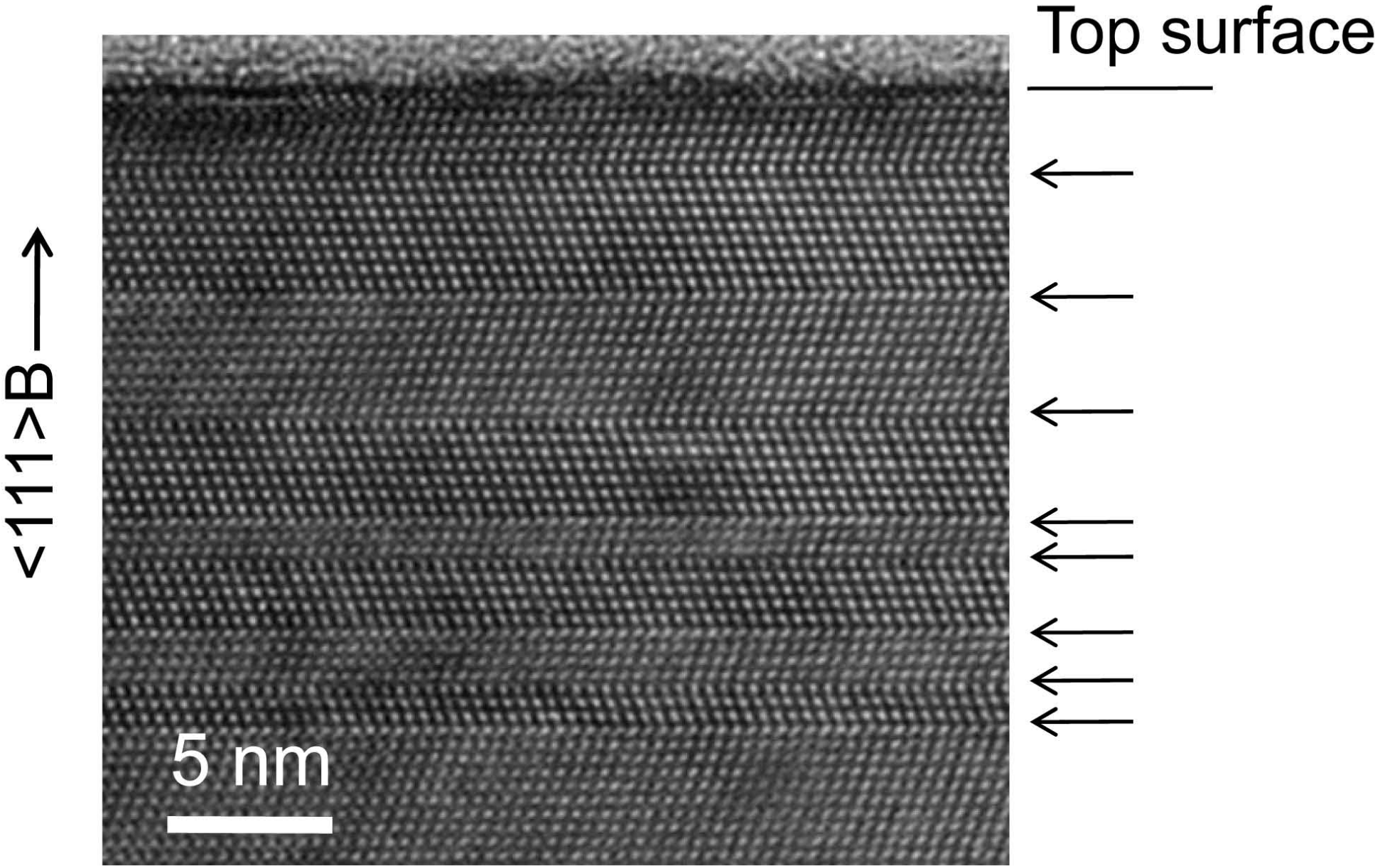

(b)
a = 0.5 μm
d0 = 80 nm
dave = 210 nm
σdiameter = 29 nm
Counts
0
10
20
30
40
0
100
200
300
400
Diameter (nm)

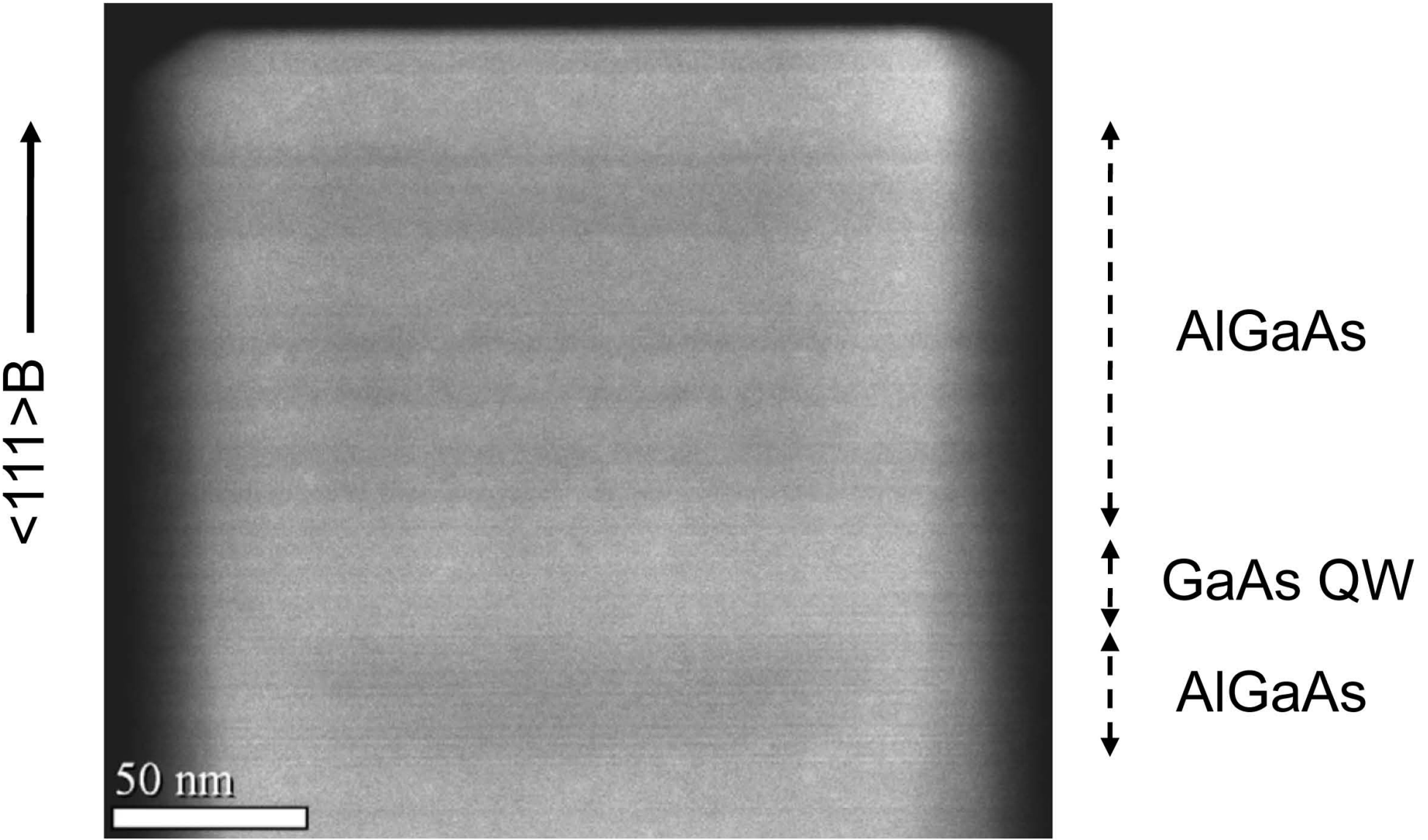

Accepter-related
emission of GaAs
GaAs
NWs
GaAs QW growth time
3 sec
5 sec
8 sec
Heterostructure NWs
PL intensity (a. u.)
Photon energy (eV)
1.4
1.2
1.0
0.8
0.6
0.4
0.2
0
1.45
1.50
1.55
1.60
1.65
PL intensity (a. u.)
6
4
2
0
3 sec
5 sec
8 sec
1.52
1.54
1.56
1.58
Photon energy (eV)

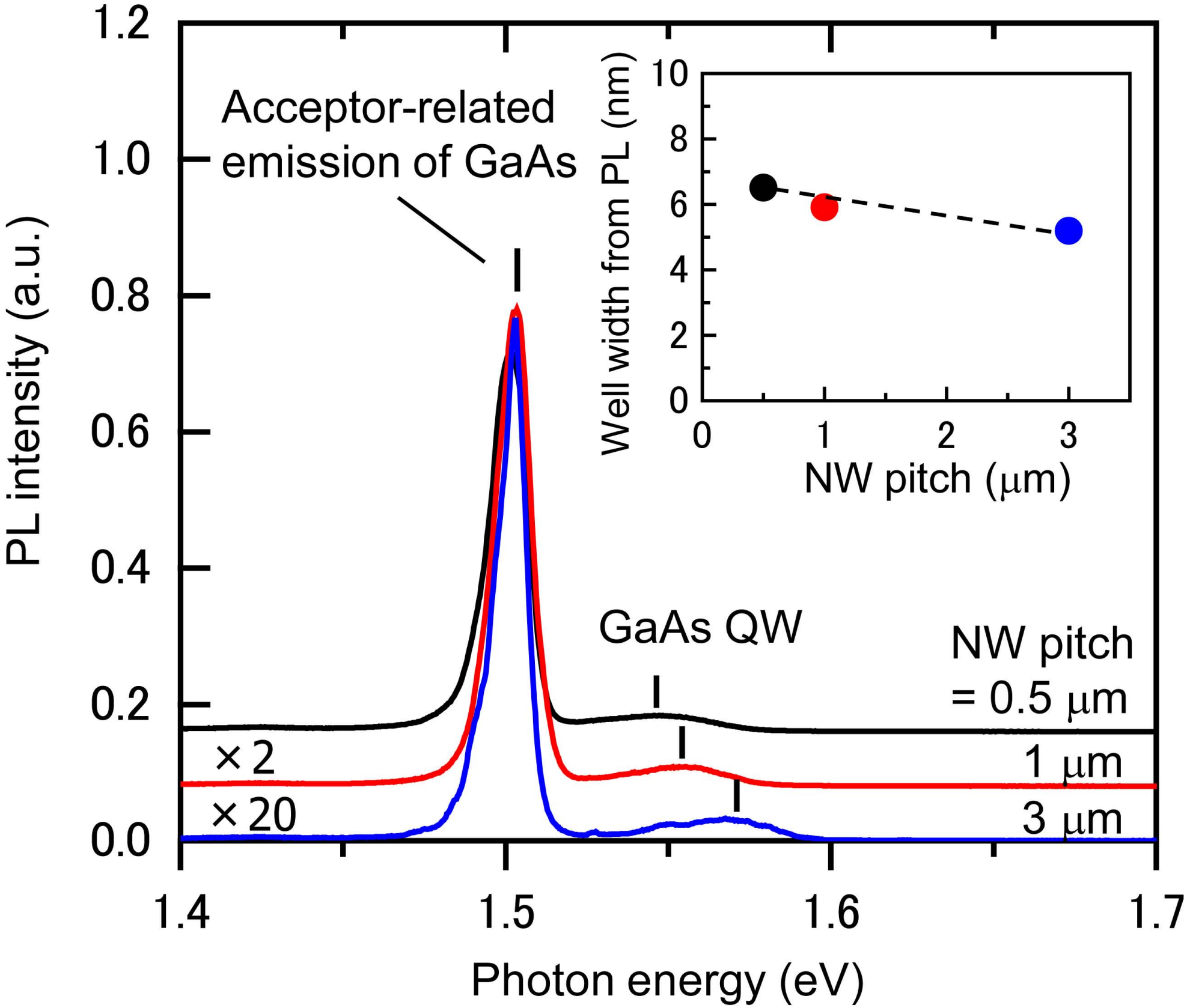

Well width L_{QW} from PL (nm)
Well width from growth rate (nm)
0
4
8
12
16
20
24
Growth time
3 sec
5 sec
8 sec
GaAs QW
Distance (nm)
0
100
200
300
400
0.0
0.1
0.2
0.3
Al composition
100 nm
<111>B


<111>B
50 nm


-1-1-1
0 0-2
Twin
-1-1 1
0 0 0
Twin
1 1-1
Twin
0 0 2
1 1 1


Top surface
<111>B
5 nm


<111>B
50 nm
AlGaAs
GaAs QW
AlGaAs


Acceptor-related
emission of GaAs
GaAs QW
NW pitch
= 0.5 μm
1 μm
3 μm
×2
×20
PL intensity (a.u.)
Photon energy (eV)
Well width from PL (nm)
NW pitch (μm)
0.0
0.2
0.4
0.6
0.8
1.0
1.2
1.4
1.5
1.6
1.7
0
2
4
6
8
10
1
2
3